Light Metals 2011 *Edited by: Stephen J. Lindsay*
TMS (The Minerals, Metals & Materials Society), 2011

INFLUENCE OF COBALT ADDITIONS ON ELECTROCHEMICAL BEHAVIOUR OF NI-FE-BASED ANODES FOR ALUMINIUM ELECTROWINNING

Vivien Singleton[1], Barry J. Welch[2], Maria Skyllas-Kazacos[1]*

[1]Centre for Electrochemical and Minerals Processing (CEMP), School of Chemical Engineering, University of New South Wales, Sydney NSW 2052 AUSTRALIA
[2]Welbank Consulting Ltd., PO Box 207, Whitianga 3542 NEW ZEALAND

Key words: inert anodes, aluminium electrolysis, Ni-Fe superalloys, corrosion resistance

Abstract

The anodic behaviour of surface-oxidised Ni-Fe-Co alloys was investigated over short-term periods of aluminium electrolysis. Additions of 10wt% Co were found to significantly improve the anodic wear resistance, due to suppression of Fe_xO formation. Anodes having cobalt contents ≥30wt% exhibited poor performance due to rapid outwards diffusion of cobalt to the reaction interface. In general, the protective ability of the pre-formed oxide scales was greatly affected by the level of porosity and surface adhesion. In electrolytes containing <4wt% Al_2O_3, catastrophic failure of the anodes was observed due to concentration polarisation at the reaction interface. Under these conditions, the metal was rapidly destroyed by a combination of dissolution and fluoridation events.

Introduction

Metals are arguably the most attractive candidates for inert anodes for the Hall-Héroult process due to their good electrical conductivity and ease of fabrication. Of the metals considered, Ni-based superalloys have shown particular promise, largely owing to:

(a) The high oxidation resistance of Ni-rich alloys; and
(b) The low solubility of Ni-containing oxides in cryolite-alumina melts [1-3].

Unfortunately, nickel and nickel-rich alloys are poorly resistant to fluoridation in the Hall cell environment. Anodes having nickel contents of ≥75wt% have been shown to undergo surface fluoridation after only a few minutes operation [4-6]. NiF_2 films have high electrical resistance and invariably cause passivation and failure of the anode.

To reduce the risk of NiF_2 formation, it is necessary to lower the nickel content of the anode by alloying with other metals. Iron has been a popular choice due to the low solubility of the nickel ferrite spinel ($Ni_xFe_{3-x}O_4$) [1]. Under oxidising conditions, Ni-Fe alloys develop layered scales consisting of one or more of the following phases [7]:

1. Iron oxides, Fe_xO:
2. Nickel oxides, Ni_xO
3. Nickel ferrite, $Ni_xFe_{3-x}O_4$

Of these, Fe_xO offers the least protection to the underlying metal from the corrosive Hall cell environment. The problem is twofold: not only are iron oxides highly soluble in the bath, but they also serve as relatively poor diffusion barriers to prevent further oxidation of the metal. Steps must therefore be taken to reduce the activity of iron in the alloy, and thereby the driving force for Fe_xO formation. It was recently suggested that this may be achieved by the addition of ternary or quaternary alloying elements [8]. In this study, the influence of cobalt additions on the anodic behaviour of Ni-Fe-based alloys is investigated.

Experimental

Anode preparation

Three compositions of Ni-Fe-Co alloy were prepared, outlined in **Error! Reference source not found.**. In all cases, the Fe:Ni mass ratio was fixed at 1:1.85. The Co concentration was set at either 10, 30 or 50 wt%. For simplicity, the alloys shall henceforth be referred to as $NiFeCo_{10}$, $NiFeCo_{30}$ and $NiFeCo_{50}$ respectively.

Table 1. Ni-Fe-Co alloy compositions

Alloy	Fe:Ni (wt)	Nominal Composition (wt%)		
		Ni	Fe	Co
$NiFeCo_{10}$	1:1.85	58.5	31.5	10
$NiFeCo_{30}$	1:1.85	45.5	24.5	30
$NiFeCo_{50}$	1:1.85	32.5	17.5	50

Alloys were prepared by arc melting using nickel, iron and cobalt lumps. Nickel (99.9wt%) and cobalt (99.99wt%) were obtained from Alfa Aesar; iron (99.9wt%) was obtained from Sigma Aldrich. The appropriate amounts of each metal were melted under reducing atmosphere (95% Ar, 5% H_2), producing button-shaped ingots of approximately 30g. The buttons were cast into rods using a copper crucible with a cylindrical mould. The rods were annealed in argon for 24h at 1100°C. The rods were machined to produce cylindrical anodes of diameter 8mm and length 10mm. The anode surfaces were abraded using 80 grit SiC paper to produce a rough surface for pre-oxidation. A female 3mm screw thread was machined into the top of each anode to facilitate connection to the cell power supply.

Pre-oxidation

Prior to electrolysis, the anodes were oxidised in air at 800°C for 24h to produce a protective semi-conducting scale. The oxidation products were identified using X-ray diffraction (XRD)

Electrolysis

The cell configuration and electrolysis procedure have been described in detail elsewhere. The laboratory-scale cell consisted of a vertical tube furnace containing a vitreous carbon crucible

cathode. Both anode and cathode were connected to the power supply using threaded stainless steel rods, sheathed using sintered alumina tubes. All electrolysis experiments were conducted at 960°C under an atmosphere of dry nitrogen. An interelectrode distance of 4cm was employed in all cases.

Two types of electrolysis experiments were performed:

(1) Electrolysis under high alumina concentration.

$NiFeCo_{10}$, $NiFeCo_{30}$ and $NiFeCo_{50}$ anodes were subjected to galvanostatic electrolysis for 2h at 0.8A/cm^2 in a bath consisting of 79.6wt% cryolite, 8.75wt% AlF_3, 4.65wt% CaF_2 and 7.0wt% Al_2O_3. To ensure stable metal pad formation, approximately 5g aluminium metal was added to the base of the crucible prior to electrolysis.

(2) Extended electrolysis without alumina replenishment

To investigate the anode behaviour under conditions of low alumina concentration, $NiFeCo_{30}$ was subjected to extended electrolysis at 0.8A/cm^2. The same initial bath composition was employed as in experiment (1). The bath was not replenished with alumina for the duration of the experiment.

Materials characterisation

Following electrolysis, the anodes were removed from the bath and allowed to cool slowly to room temperature. Once cool, the anodes were immediately mounted in epoxy resin to prevent absorption of moisture. The mounted specimens were gently abraded using fine-grit SiC paper to expose the anode/bath interface. XRD analysis was carried out using a Philips X'Pert PRO Materials Research Diffractometer with resolution =0.02°2θ, divergence slit =¼°, anti-scatter slit =½° and 0.04 radian soller slits in the incident and receiving positions. A mono-capillary was fitted to the instrument for incident beam conditioning and focusing.

The carbon crucible cells containing frozen bath were potted in epoxy resin and sliced in half to reveal a vertical cross-section. Energy dispersive x-ray spectroscopy (EDX) analysis was performed on selected areas of the crucible cross-section.

Results and discussion

Pre-oxidation

Anodes were pre-oxidised at 800°C for 24 h in air, producing adherent scales approximately 10-30μm thick. To assess the extent of oxidation, the anodes were weighed before and after oxidation to determine the net mass gain. For comparison, a binary Ni-Fe alloy having the equivalent Fe:Ni mass ratio (1:1.85) was oxidised under the same conditions. The results are shown in Figure 1.

It is clear that oxidation resistance decreases strongly with additions of ≥30wt% Co. Interestingly, addition of 10wt% Co results in an increase in oxidation resistance compared to the binary alloy. It is possible that the addition of small amounts of cobalt to the alloy significantly reduces the iron activity, lowering the driving force for Fe diffusion through the scale according to Fick's laws [9].

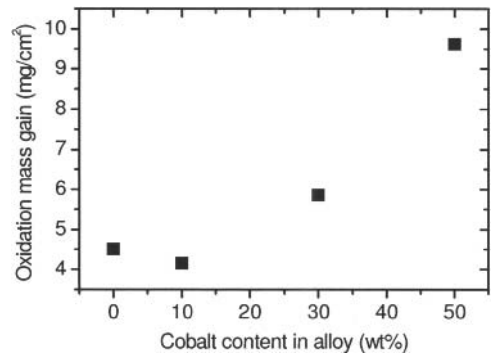

Figure 1. Mass gain versus cobalt content for Ni-Fe-Co alloys oxidised at 800°C for 24h.

Unfortunately, there is very little information available in the literature about the oxidation behaviour of Ni-Fe-Co alloys. Previous studies have largely focussed on Fe-rich systems such as Kovar [10] or maraging steels [11-13].

Oxidation products were identified using XRD analysis. X-ray diffraction spectra are shown in Figure 2. Scales on alloys having ≥30wt% Co were cobalt-rich, consisting principally of Co_3O_4, $Ni_xCo_{3-x}O_4$ and $Co_xFe_{3-x}O_4$. In the case of $NiFeCo_{10}$, the major oxidation product was the nickel ferrite spinel ($Ni_xFe_{3-x}O_4$), with small amounts of Co_3O_4. Cobalt (II) oxide was observed only on $NiFeCo_{50}$.

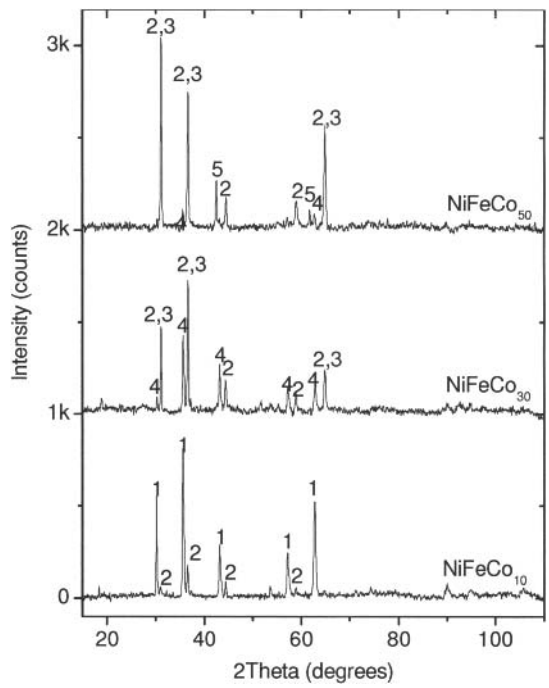

Figure 2. XRD spectra of oxidation products on Ni-Fe-Co alloys following 24h oxidation at 800°C in air. 1-$Ni_xFe_{3-x}O_4$, 2-Co_3O_4, 3-$Ni_xCo_{3-x}O_4$, 4-$Co_xFe_{3-x}O_4$, 5-CoO.

It has been well documented that hematite (Fe_2O_3) is formed on Ni-Fe alloys containing as little as 15wt% Fe under the chosen conditions [7, 14-15]. In the present study, no perceptible amounts of Fe_2O_3 were observed following pre-oxidation. It is likely that Fe_2O_3 formation is suppressed due to preferential oxidation of cobalt, resulting in scales containing cobalt oxides and cobaltite spinels. Of course, it remains to be seen whether these cobalt-rich phases offer any advantages as protective barriers during electrolysis. Promisingly, $NiFeCo_{10}$ appears to offer the dual advantages of high oxidation resistance and a strong preference for nickel ferrite formation.

Electrolysis under high alumina concentration

Galvanostatic electrolysis was performed using pre-oxidised Ni-Fe-Co anodes for 2h at 0.8A/cm^2 (absolute current = 1.41A). The initial alumina concentration in the electrolyte was a nominal 7.0wt% (the saturation point was estimated as 7.9wt% using models developed by Grjotheim and Welch [16]). Assuming a 90% current efficiency, it was predicted that the alumina concentration would decrease by no more than 1wt% throughout the experiment.

Potential versus time plots for each anode are shown in Figure 3. Potentials are reported with reference to the aluminium deposition potential, with the graphite/aluminium cathode serving as a quasi-reference electrode. It should be noted that the reported cell voltages include ohmic contributions. Since the electrical conductivity of the bath does not change dramatically with Al_2O_3 concentration [17-19] and the cathode reaction does not change, it may be reasonably assumed that fluctuations in the cell potential reflect changes in the anode processes or condition. The electrochemical potential was estimated by approximating the voltage contributions due to non-faradaic processes. The total cell voltage is given by Equation 1:

$$E_{cell} = E_{anode} - E_{cathode} + iR_{anode} + iR_{cathode} + iR_{bath} + iR_{ext} + \eta \quad (1)$$

Where	E_{anode}	is the reversible anodic potential
	$E_{cathode}$	is the reversible cathodic potential
	R_{anode}	is the anodic resistance
	$R_{cathode}$	is the cathodic resistance
	R_{bath}	is the bath and bubble layer resistance
	R_{ext}	is the resistance due to external components such as leads and connections
	i	is the cell current
	η	is the overvoltage

Additional voltage requirements due to anode and cathode and resistances are expected to be low: the individual materials resistivities are in the order of 1-10μΩ.cm at the operating temperature. Voltage requirements due to contact resistances were estimated to be in the order of 0.1V. The bath resistivity was estimated at 0.5Ω.cm using models developed by Híveš et al. [17-19], contributing an additional 0.15V. The overpotential at 0.8A/cm^2 was estimated between 0.3-0.5V, based on data published by Thonstad *et al* [20]. The remaining potential difference, representing the electrochemical potential, changes considerably depending on the anode material and condition. In most cases, potentials above the oxygen evolution potential (2.2V vs AlF_3/Al) are observed. As such, we can be reasonably confident that oxygen evolution is one of the primary anodic reactions.

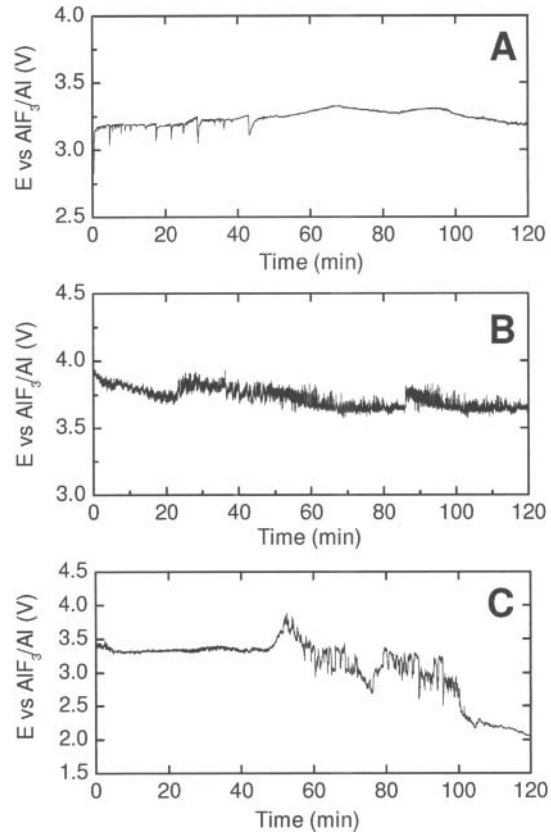

Figure 3. Potential vs. time plots for: A-$NiFeCo_{10}$, B-$NiFeCo_{30}$ and C-$NiFeCo_{50}$ anodes. Temperature: 960°C, current density: 0.8A/cm^2, interelectrode distance: 4cm.

Table 2. List of possible reactions on Ni-Fe-Co anodes in cryolite-alumina melts

Reaction	E at 1000°C (V)		Ref
	Theoretical‡	Measured	
$3Ni + 2AlF_3 \rightarrow 3NiF_2 + 2Al$	1.69	1.40	[21]
$3Ni + Al_2O_3 \rightarrow 3NiO + 2Al$	1.55	1.48†	[4]
$3Fe + 2AlF_3 \rightarrow 3FeF_2 + 2Al$	1.27	0.85	[21]
$3Fe + Al_2O_3 \rightarrow 3FeO + 2Al$	1.26	-	
$2Fe + Al_2O_3 \rightarrow Fe_2O_3 + 2Al$	1.35	1.16†	[4]
$9Fe + 4Al_2O_3 \rightarrow 3Fe_3O_4 + 8Al$	1.27	-	
$3Co + 2AlF_3 \rightarrow 3CoF_2 + 2Al$	1.52	1.25	[21]
$3Co + Al_2O_3 \rightarrow 3CoO + 2Al$	1.45	-	
$9Co + 4Al_2O_3 \rightarrow 3Co_3O_4 + 8Al$	1.65	-	
$2Al_2O_3 \rightarrow 3O_2 + 4Al$	2.19	2.20	[22]
$2AlF_3 \rightarrow 3F_2 + 2Al$	4.07	-	

‡ Calculated using HSC software, licensed to Outokumpu Research.
† Measured at 970°C

Table 2 provides a non-exhaustive list of possible cell reactions and their theoretical and measured potentials at 1000°C. While oxygen evolution is likely to be the primary anodic reaction at most stages of electrolysis, it is probable that a number of other reactions occur – most notably, oxidation and fluoridation of the anode metal. It is clear that the nature of the primary anodic

reaction is significantly influenced by the relative activities of Al_2O_3 and AlF_3 in the melt. Under high Al_2O_3 activity, oxygen-rich products – such as metal oxides and oxygen gas – are likely to dominate. Under low Al_2O_3 activity, fluoridation reactions dominate, usually leading to accelerated anode wear and in most cases, passivation. This indicates why it is necessary to maintain a high alumina concentration during cell operation with inert anodes. As well as reducing the dissolution rate of the protective oxide scale, a high alumina activity suppresses fluoridation reactions, which in turn, extends the lifetime of the anode. Of course, without the assistance of additional analytical techniques, it is difficult to speculate about the types of reactions occurring at the anode surface.

Figure **3** suggests that $NiFeCo_{10}$ and $NiFeCo_{30}$ maintained steady oxygen evolution for the duration of the experiment. In each case, stable anodic voltages were observed – approximately 3.25V and 3.75V respectively. It is unclear why a significantly higher voltage was observed for $NiFeCo_{30}$. It is possible that the thicker pre-formed scale on $NiFeCo_{30}$ causes a higher anodic resistance. Alternatively, the formation of an electrically resistive species may have occurred at the anode surface.

For $NiFeCo_{10}$, intermittent rapid drops in potential were observed during the first hour of electrolysis. The potential drops can be seen as small spikes on the voltage plot in Figure 3. In each case, the potential drops rapidly by 0.1-0.2V, then returns slowly to the steady-state voltage over 20-30sec. It is likely that these events represent spallation of parts of the scale from anode surface, possibly as a result of gas evolution. The potential returns to the steady-state value as the oxide is re-formed *in situ*. Interestingly, the spalling events cease in the final hour of electrolysis, possibly indicating complete destruction of the original scale. For improved anode performance, it may be necessary to significantly reduce the frequency of spalling by improving the scale adhesion.

$NiFeCo_{50}$ performed poorly during electrolysis, exhibiting highly unstable behaviour. For the first 45min of the experiment, the anode maintained a steady potential of approximately 3.35V. Following this, the voltage increased sharply to ~4V, then declined slowly to ~2.1V with significant noise. Oxygen evolution ceases in the last 20min of electrolysis as the potential drops below 2.2V. It is likely that the primary anodic reaction during this period is metal dissolution.

Following electrolysis, the anodes were mounted in epoxy resin and sliced vertically to reveal a cross-section of the electrode centre. Optical micrographs of the cross-sections are shown in Figure 4. While no significant changes in the anode dimensions were observed, it was clear that the protective scales had become severely damaged during the experiment. In all cases, the scales had delaminated from the anode surface, causing massive bath penetration and metal wear. The bath appears to have penetrated 500-800μm into the alloy, leaving the metal etched at the grain boundaries. Importantly, it appears to be the action of the bath, and not thermal shock due to re-heating of the scales, that causes delamination of the oxide layer. Inspection of the portion of the anodes which had not been in contact with the bath showed that the oxide scales in these regions were still well adhered to the metal.

The relative thicknesses of the remaining scales offer information about the solubilities of the oxidation products in the cryolite-alumina bath (or, more accurately, the relative rates of oxide formation and dissolution). Despite having significantly lower oxidation resistance, the cobalt-rich anodes $NiFeCo_{30}$ and $NiFeCo_{50}$ have relatively thin reaction scales (50-200μm). In comparison, $NiFeCo_{10}$ has a thick scale (400-500μm): over 25 times greater than its starting thickness, as assessed by optical microscopy. This suggests that oxide phases formed on $NiFeCo_{10}$ – principally $Ni_xFe_{3-x}O_4$ and NiO – are significantly less soluble than cobalt-containing oxides.

XRD analysis was performed on the scale/bath interfaces following electrolysis. The spectra are shown in Figure 5. It is clear that the surface compositions have changed considerably over the course of electrolysis. In particular, there is a notable absence of cobalt-rich phases (Co_3O_4, CoO, $Co_xFe_{3-x}O_4$, $Ni_xCo_{3-x}O_4$) in preference for nickel-rich phases (NiO, $Ni_xFe_{3-x}O_4$). This reflects the significantly lower solubility of Ni-based oxides in the electrolyte.

Iron (II) fluoride, FeF_2, was found in significant quantities on the surface of the $NiFeCo_{30}$ anode. Most metal fluorides are poorly conductive, and can contribute to anode passivation if deposited in significant concentrations on the anode surface. The average anode potential during electrolysis was not unusually high (see Figure 3), suggesting that FeF_2 has minimal effect on the scale conductivity when present in these concentrations.

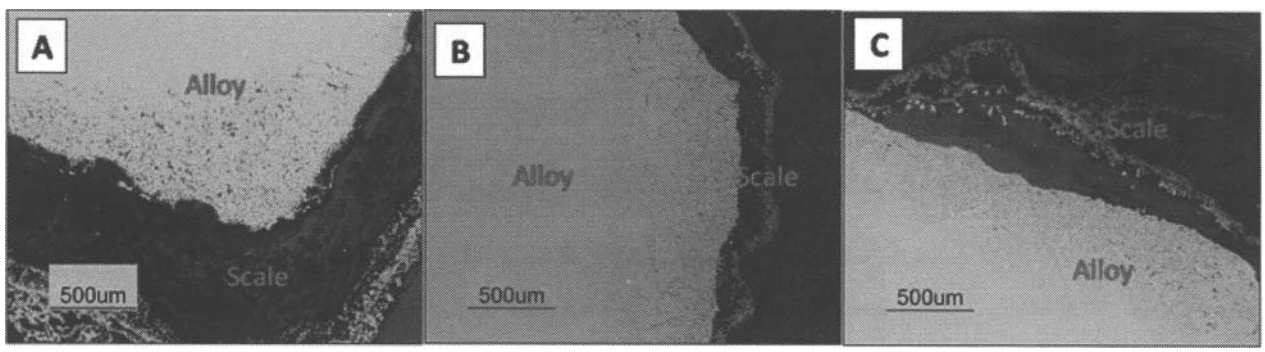

Figure 4. Optical micrographs of Ni-Fe-Co anode cross-sections following 2h electrolysis. A-$NiFeCo_{10}$, B-$NiFeCo_{30}$, C-$NiFeCo_{50}$.

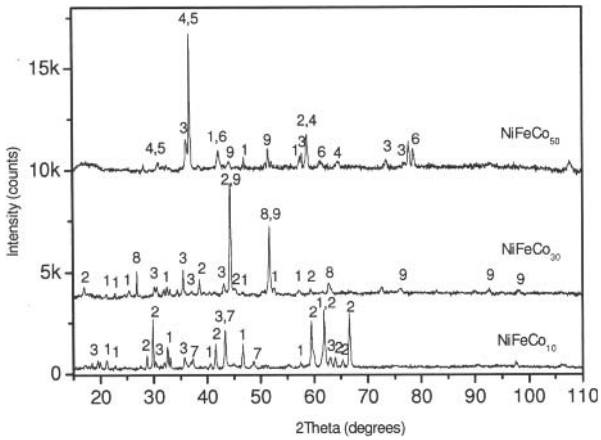

Figure 5. XRD spectra of scale/bath interface on Ni-Fe-Co anodes following 2h electrolysis at 0.8A/cm^2. 1-Cryolite, 2-Chiolite, 3-$Ni_xFe_{3-x}O_4$, 4-Co_3O_4, 5-$CoAl_2O_4$, 6-CoO, 7-NiO, 8-FeF_2, 9-$FeNi_3$.

Extended electrolysis without alumina replenishment

Extended electrolysis using pre-oxidised $NiFeCo_{30}$ was terminated after 4h due to catastrophic failure of the anode. Figure 6 shows the potential versus time plot for the cell. The anode maintained a steady potential of approximately 4.5V for the first 3 hours of electrolysis. It can be reasonably assumed that oxygen evolution occurs during this time. In the final hour of electrolysis, the potential increased steadily to >10V. This indicates a dramatic rise in anode resistivity, almost certainly caused by fluoridation of the metal.

Based on an assumed current efficiency of 90%, the alumina depletion rate was predicted as approximately 1.1g/hr, or 1.2wt%/hr. Assuming the prediction is accurate, the bulk alumina concentration at the onset of anode failure (approx. 3h electrolysis time) was around 3.4wt%. However, it is likely that the oxide concentration at the electrode surface is much lower, giving rise to concentration polarisation and the onset of an anode effect. It has been shown that the solubility of iron and nickel oxides is 3-10 times higher in baths containing 3wt% Al_2O_3 than 7wt% Al_2O_3 [3, 23]. Under these conditions, complete destruction of the protective scale is anticipated. As a consequence, the anode metal becomes exposed to the bath and is subsequently dissolved.

Following electrolysis, the anode was cooled and removed from the cell for visual inspection. As expected, the dimensions of the anode had been significantly reduced, indicating wholesale dissolution of the metal in the bath. In comparison, the $NiFeCo_{30}$ anode dimensions were virtually unchanged after 2h electrolysis. Hence, it is clear that the majority of anode wear occurs in the 2-4h period, when the alumina concentration drops below 5wt%.

XRD analysis was performed on the remaining part of the destroyed anode. It was found that the anode consisted almost entirely of metal oxide species and solidified bath material. This helps to explain the high anodic resistance observed in the final hour of electrolysis. Interestingly, despite the alloy's high initial cobalt concentration, the remaining part of the anode contained no detectable amounts of cobalt oxide. Instead, nickel-rich oxides were observed, including NiO and $Ni_xFe_{3-x}O_4$. From these results, it is clear that cobalt oxides have relatively high solubility in the bath.

Following electrolysis, the graphite crucible cathode was potted in epoxy resin and sliced in half to reveal a vertical cross-section of the cell. A photograph of the halved cell is shown in Figure **7**. To gain information about the distribution of elements within the cell, EDX point analysis was performed on selected areas of the cross-section. There are several regions of interest: first, the "U" shaped area of dark material marked 3 on the photograph. This area appears to represent regions of reduced metal which have been deposited on the sides of the crucible, and are trickling down toward the large mass of metal at the base of the cell. Interestingly, the EDX spectrum indicates that the metal deposit does not contain appreciable amounts of aluminium, but is instead composed of iron from the anode and small amounts of chromium from the stainless steel connecting rod.

The lump of reduced metal at the base of the cell is approximately twice the size of the aluminium button added to the crucible prior to electrolysis. The round – almost circular – shape of the deposit indicates the very high surface tension between the liquid aluminium pad and the graphite crucible. The deposit appears to consist of two distinct regions: an outer, more porous region and an inner dense region. EDX analysis revealed that the outer region is predominantly aluminium, while the inner region is represented by re-deposited metal from the dissolved anode. At the cell operating temperature of 960°C, the intermetallic compounds of nickel, iron and cobalt are well below their liquidus temperatures. Re-deposition of the dissolved anode metals would result in a solid product, having much higher density than liquid aluminium. As a consequence, we see most of the metal contaminants being segregated from the aluminium product.

Interestingly, the lump of re-deposited anode metal appears to contain only a small amount of cobalt. Clearly, the Kα peak intensities of the EDX spectrum (Point 1 in Figure **7**) are not proportional to the ratio of Ni, Fe and Co in the original alloy. Further EDX analysis revealed that cobalt was undetectable in other regions of the crucible. Furthermore, the XRD analysis of the damaged anode revealed virtually no cobalt remained in the alloy. A crude mass balance for the system would suggest that a

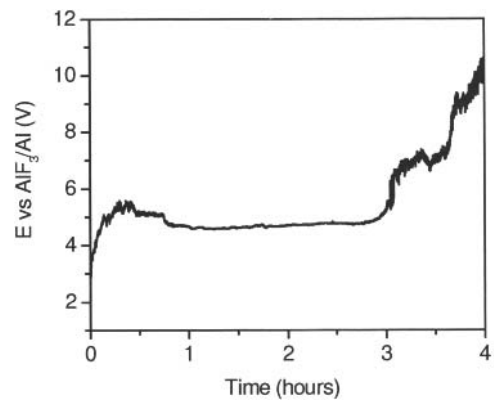

Figure 6. Potential versus time plot for oxidised $NiFeCo_{30}$ anode, subjected to extended electrolysis at 0.8A/cm^2 without alumina replenishment.

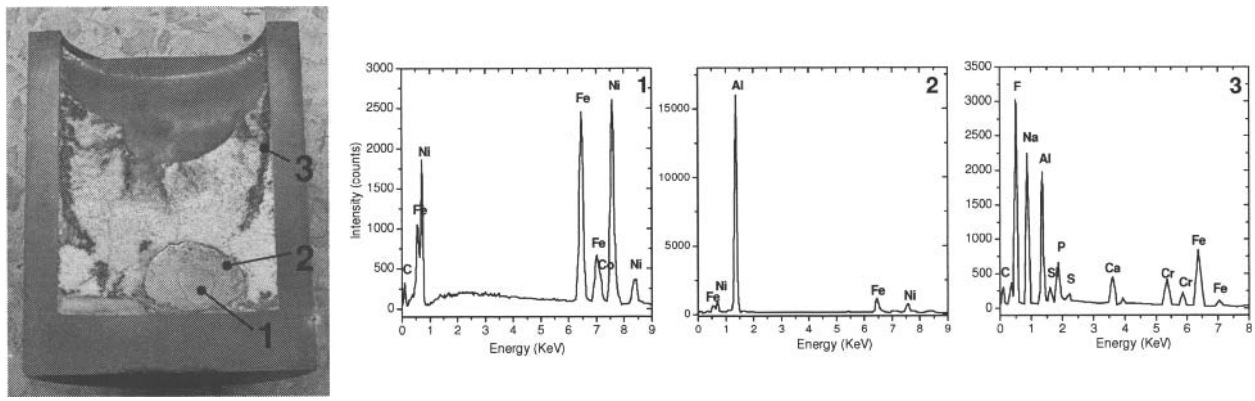

Figure 7. Left- photograph of crucible cross section following 4h electrolysis without alumina replenishment. Right- EDX spectra of selected points on the cell cross section.

significant amount of cobalt has been lost, probably in the form of a volatile product.

Conclusions

The anodic behaviour of pre-oxidised Ni-Fe-Co alloys was investigated during short-term aluminium electrolysis. A general correlation exists between the oxidation resistance of the anode metal and the short-term anode performance. In particular, anode compositions with a preference for $Ni_xFe_{3-x}O_4$ formation must be considered promising, owing to the very low solubility of the spinel in the electrowinning bath. It was demonstrated that the preference for $Ni_xFe_{3-x}O_4$ formation can be strongly increased by the addition of 10wt% Co to the Ni-Fe system. Alloys containing ≥30wt% Co performed poorly due to high corrosion rate and relatively high solubility of cobalt-containing oxides.

Visual inspection of the anodes following electrolysis showed that all alloys were inadequately protected by the pre-formed oxide scale. Bath penetration through pores and defects in the scale was shown to result in irreversible anode damage. Therefore, there is a strong need to improve scale adhesion and compactness, possibly by appropriate physical pre-treatment of the anode surface or incorporation of small quantities of rare earth elements to the alloy. The need to maintain alumina concentration at close to saturation was highlighted during extended electrolysis.

References

[1] D.H. DeYoung, *Light Metals 1986*, R.E. Miller Editor, TMS, Warrendale PA (1986) 299.

[2] S. Pietrzyk and R. Oblakovski, *Light Metals 1999*, C.E. Eckert Editor, TMS, Warrendale PA (1999) 407.

[3] T.E. Jentoftsen, O.-A. Lorentsen, E.W. Dewing, G.M. Haarberg, and J. Thonstad, *Metall. Mater. Trans. B*, 33 (2002) 901.

[4] P.G. Russell, *J. Appl. Electrochem.*, 16 (1986) 147.

[5] E.V. Antipov, A.G. Borzenko, V.M. Denisov, A.Y. Filatov, V.V. Ivanov, S.M. Kazakov, P.M. Mazin, V.M. Mazin, V.I. Shtanov, D.A. Simakov, G.A. Tsirlina, S.Y. Vassiliev, and Y.A. Velikodny, *Light Metals 2006*, T.J. Galloway Editor, TMS, Warrendale PA (2006) 403.

[6] D.A. Simakov, E.V. Antipov, M.I. Borzenko, S.Y. Vassiliev, Y.A. Velikodny, V.M. Denisov, V.V. Ivanov, S.M. Kazakov, Z.V. Kuzminova, A.Y. Filatov, G.A. Tsirlina, and V.I. Shtanov, *Light Metals 2007*, M. Sørlie Editor, TMS, Warrendale PA (2007) 489.

[7] R.T. Foley, *J. Electrochem. Soc.*, 109 (1962) 1202.

[8] B.J. Welch, *Light Metals 2009*, TMS, Warrendale PA (2009) 971.

[9] A. Fick, *Phil. Mag.*, 10 (1855) 30.

[10] D.W. Luo and Z.S. Shen, *Acta Metall. Sinica*, 21 (2008) 409.

[11] I.E. Klein, A.V. Yaniv, and J. Sharon, *Oxidation of Metals*, 16 (1981) 99.

[12] J. Wu, L. Zhang, J. Zhou, and Y. Xu, *J. Mater. Sci. Tech.*, 16 (2000) 509.

[13] B.-S. Kim, B.-G. Kim, H.-W. Lee, and W.-S. Chubg, *Metals and Materials International*, 8 (2002) 367.

[14] G.L. Wulf, T.J. Carter, and G.R. Wallwork, *Corr. Sci.*, 9 (1969) 689.

[15] I.A. Menzies and J. Lubkiewicz, *J. Electrochem. Soc.*, 117 (1970) 1539.

[16] K. Grjotheim and B.J. Welch, *Aluminium Smelter Technology: A Pure and Applied Approach*. 1980, Düsseldorf: Aluminium-Verlag.

[17] J. Híveš, J. Thonstad, Å. Sterten, and P. Fellner, *Light Metals 1994*, U. Mannweiler Editor, TMS, Warrendale PA (1994) 187.

[18] J. Híveš, J. Thonstad, Å. Sterten, and P. Fellner, *Metall. Mater. Trans. B*, 27B (1996) 255.

[19] J. Thonstad, P. Fellner, G.M. Haarberg, J. Híveš, H. Kvande, and Å. Sterten, *Aluminium Electrolysis: Fundamentals of the Hall-Héroult Process*. 3rd ed. 2001, Düsseldorf: Aluminium-Verlag.

[20] J. Thonstad, A. Kisza, and J. Hives, *Light Metals 2006*, T.J. Galloway Editor, TMS, Warrendale PA (2006) 373.

[21] L. Cassayre, P. Chamelot, L. Arurault, and P. Taxil, *J. Appl. Electrochem.*, 35 (2005) 999.

[22] J. Thonstad, *Electrochim. Acta*, 13 (1968) 449.

[23] T. Utigard, *Light Metals 1993*, S.K. Das Editor, TMS, Warrendale PA (1993) 319.